Aeroelastic Behavior of a Laminar Wing in Transonic Flow

Michael Fehrs(✉), Sebastian Helm, Christoph Kaiser, and Thomas Klimmek

DLR, Institute of Aeroelasticity, 37073 Göttingen, Germany
michael.fehrs@dlr.de,
https://www.dlr.de/ae/

Abstract. A laminar wing test case for the flutter behavior in transonic flow with free boundary layer transition is presented. The DLR-AE-L1 airfoil and wing are designed to serve as an aeroelastic testbed to develop a better understanding for the effect of boundary layer transition on flutter stability. Coupled CFD-CSM simulations are used to determine the flutter onset in a transitional and a fully turbulent flow. It is found that flutter occurs at lower stagnation pressures for the transitional flow, which is in accordance with earlier research on laminar airfoils.

Keywords: Laminar wing · Boundary layer transition · CFD-CSM coupling · Transonic flutter

1 Introduction

Natural laminar flow airfoils and wings allow more ecologic and economic transport aircraft by reducing the friction drag during cruise flight significantly. Laminar flow control by active and passive means is well understood from an aerodynamic point of view, but aeroelastic effects have not been considered sufficiently yet [1]. The partly laminar boundary layer flow alters the lift and moment acting on the wing as the displacement thickness of the boundary layer is changed. In transonic flow, changes in the shock location and strength have the potential to introduce shock-induced boundary layer separations that can affect the flutter behavior directly. In addition, any partial or complete loss of laminarity introduces aerodynamic non-linearities, which in turn might affect the dynamic aeroelastic stability.

The objective of this paper is to introduce an airfoil and wing geometry as an aerodynamic and aeroelastic testbed that can be distributed without any restrictions[1]. The airfoil is mainly designed to attenuate Tollmien-Schlichting (TS) transition. A small leading-edge sweep angle is used to prevent crossflow transition. There is no intention to design a state-of-the-art laminar airfoil and wing that serves all needs of a modern transport aircraft design as it is done by other research groups [2,3].

[1] Please contact first author.

A. Dillmann et al. (Eds.): STAB/DGLR Symposium 2020, NNFM 151, pp. 164–173, 2021.
https://doi.org/10.1007/978-3-030-79561-0_16

2 Methods

2.1 ModGen: Geometry and Structural Model

The wing geometry and structural model are created with the DLR computer program ModGen. ModGen is mainly designed to generate finite element models for the load carrying structure of wing-like and fuselage components of an aircraft [4]. As ModGen is setting up parametrically defined geometry models as a prerequisite for the finite element model generation, these geometry models of the outer wing geometry can also be used for the CFD mesh generation.

2.2 DLR TAU-Code: Transition Prediction

The flow field is computed with the DLR TAU-Code [5]. Boundary layer transition is considered based on the correlation-based γ transition model [6] and linear stability theory with the DLR transition module [7,8]. The γ transition model is used for most of the steady and unsteady computations. It is advantageous for unsteady computations as the transition prediction is performed at each inner iteration of each physical time step and on each computational grid point.

As the γ model is not able to predict crossflow transition, the e^N method of the DLR transition module is used to confirm the transition prediction by the γ transition model for the steady flow computations. The SST $k-\omega$ turbulence model is used for all fully turbulent computations. It is also used as the underlying turbulence model for both transition prediction methods.

2.3 FlowSimulator: CFD-CSM Coupling

The CFD-CSM coupling is performed within the FlowSimulator environment which is designed to enhance CFD-related multidisciplinary analysis [9]. The time-integration is conducted in a co-simulation exchanging structural deformations and aerodynamic forces at each time step. The mode shapes are mapped onto the CFD grid to account for displacements of the structure by mesh deformation and the structural displacements are obtained by employing the Newmark-beta method [10].

3 Results

3.1 Aerodynamics

Airfoil: The Boeing HSNLF airfoil is chosen [11] as the baseline geometry for the airfoil design. The airfoil is supposed to provide a large extent of laminar flow and low shock wave losses at transonic Mach numbers. Laminar boundary layer flow of at least up to 50% to 60% of the chord length is expected on the upper surface within the design Reynolds number range of $Re = 15 \cdot 10^6$ to $30 \cdot 10^6$ for $c_l = 0.5$ at $M = 0.78$.

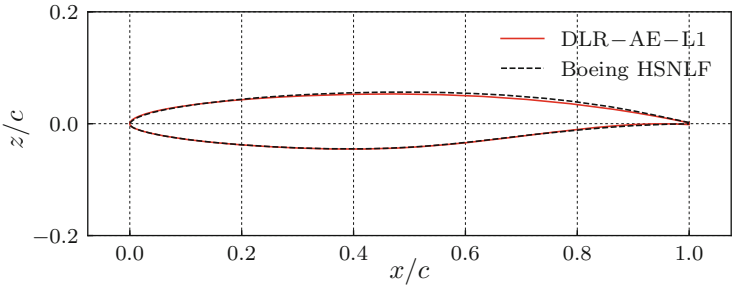

Fig. 1. DLR-AE-L1 and Boeing HSNLF Airfoil: geometry

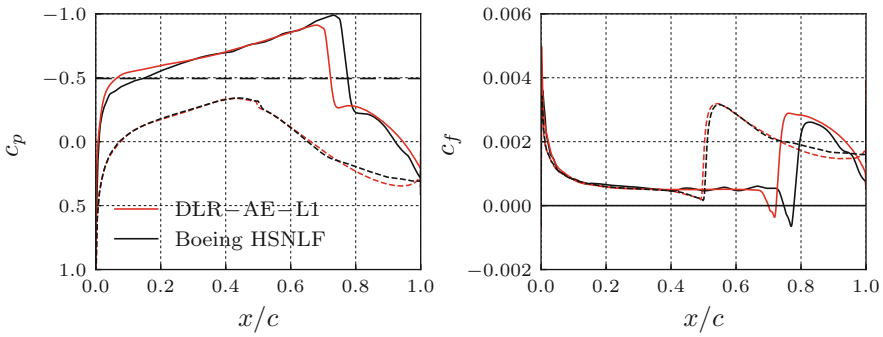

Fig. 2. DLR-AE-L1 and Boeing HSNLF Airfoil: pressure and skin friction coefficient distribution at $c_l = 0.5$, $M = 0.78$, $Re = 15 \cdot 10^6$; full line: upper surface, dashed line: lower surface

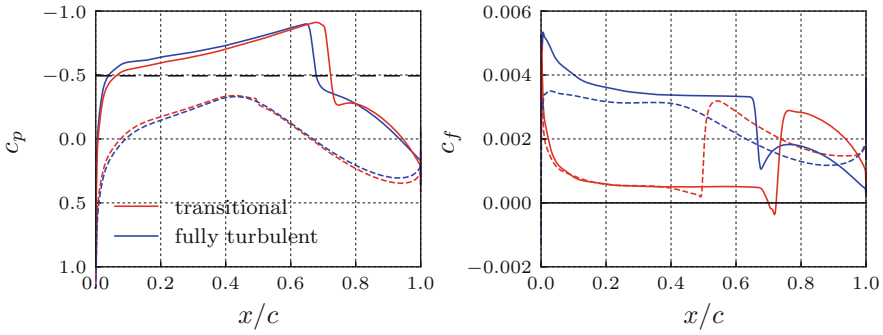

Fig. 3. DLR-AE-L1 Airfoil: pressure and skin friction coefficient distribution at $c_l = 0.5$, $M = 0.78$, $Re = 15 \cdot 10^6$ for the transitional and fully turbulent flow; full line: upper surface, dashed line: lower surface

The Boeing HSNLF is not used directly as it is not possible to recreate the design pressure distribution. In addition, the documented airfoil data do not provide a smooth enough surface for high Reynolds number computations.

The design condition for the Boeing HSNLF of $Re = 15 \cdot 10^6$, $c_l = 0.5$, $M = 0.78$ are kept for the DLR-AE-L1. The airfoil coordinates are modified to move the shock location upstream by reducing the curvature of the upper surface. In addition, the nose geometry is changed to reduce the favorable pressure gradient on the suction side downstream of $x/c \approx 0.1$ to attenuate the growth of crossflow instabilities. The lower aft section is modified to produce more lift by an increased curvature. The modified point data is smoothed using a b-spline interpolation. It is found that the resulting airfoil coordinates are well represented in geometry tools (ModGen), grid generators (ANSYS ICEM, Centaur), and result in a sufficiently smooth pressure distribution at the design Reynolds number.

Figure 1 shows the DLR-AE-L1 airfoil and the Boeing baseline geometry. Figure 2 shows the pressure and skin friction coefficient distribution at $Re = 15 \cdot 10^6$, $c_l = 0.5$, $M = 0.78$. The γ transition model is used for transition prediction. The turbulence level is set to $Tu = 0.05\%$, which represents a very quiet wind tunnel or free flight conditions. The shock on the upper surface is successfully moved upstream and the corresponding boundary layer separation is weakened.

Figure 3 shows the pressure and skin friction coefficient distribution for the DLR-AE-L1 in a transitional and a fully turbulent flow at the same flow conditions as above. The shock location is located more aft for the transitional flow, as the displacement thickness decreases in the partly laminar flow.

Wing: The wing with a semi-wingspan of $b/2 = 1.6\,\text{m}$ and no twist has a leading edge sweep angle of $\Lambda_{LE} = 20°$, a root chord length of $c_{root} = 0.5\,\text{m}$, a tip chord length of $c_{tip} = 0.15\,\text{m}$, and a taper ratio of $\lambda = c_{tip}/c_{root} = 0.3$. For simplicity, the airfoil sections are aligned in flow direction. The geometric parameters give a mean aerodynamic chord of $c_{mac} = 0.35641\,\text{m}$.

The computational grid consists of a structured surface mesh with 350 nodes in chord and 250 in span direction. The prism boundary layer grid consists of 85 layers, for which the maximum y^+ value of the first grid cell is about 0.5 for the investigated flow conditions. The overall grid contains about $17 \cdot 10^6$ nodes. No systematic grid convergence study is performed yet but it is checked that the transition model behaves well within the transition region.

Figure 4 shows the angle of attack, moment, and drag coefficient for a constant lift coefficient of $C_L = 0.5$ with increasing Mach number at $Re_{mac} = 15 \cdot 10^6$. The variation of the angle of attack to maintain the desired lift coefficient and the change in the moment coefficient with Mach number are much more pronounced for the transitional flow. As the drag divergence Mach number is approached, the drag coefficients of the transitional flow remain beneath the drag for the fully turbulent flow. The drag benefit due to lower skin friction is larger than the drag penalty due to a stronger shock and larger boundary

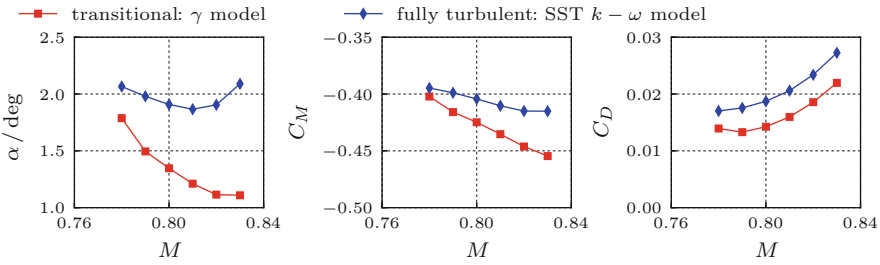

Fig. 4. DLR-AE-L1 Wing: Angle of attack, moment, and drag coefficient for increasing Mach numbers at $C_L = 0.5$, $Re_{mac} = 15 \cdot 10^6$

layer separation. At higher Mach numbers, no steady solution is found for the target lift coefficient, which is most likely caused by shock buffet due to shock-boundary-layer interaction.

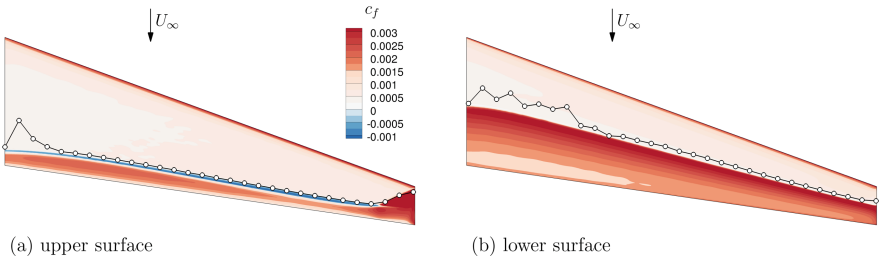

(a) upper surface (b) lower surface

Fig. 5. DLR-AE-L1 Wing: skin friction coefficient distribution computed with the γ transition model and transition line from the stability code LILO

Figure 5 shows the skin friction coefficient distribution computed with the γ model at $C_L = 0.5$, $M = 0.82$, $Re_{mac} = 15 \cdot 10^6$. The transition location is found at the main increase in skin friction coefficient. In addition, the transition location obtained with the TAU transition module [7,8] with the boundary layer code COCO and the stability code LILO for critical incompressible N factors of $N_{TS} = 11.8$ and $N_{CF} = 8.4$ is shown by the line in Fig. 5. The transition locations predicted by both methods match well on both the upper and lower surface of the wing. The stability code predicts a combination of crossflow and Tollmien-Schlichting transition towards the wing root, but the transition location does not shift much upstream. It should be noted that the critical N factors are rather low compared to a turbulence level of $Tu = 0.05\%$. Due to the overall dominance of TS transition, it is assumed that the γ model can be used for transition prediction for these flow conditions.

3.2 Structural Model

For investigating the differences between the flutter behavior in a transitional and a fully turbulent flow, the structural model is tailored to exhibit flutter for the examined range of aerodynamic parameters at realistic wind tunnel stagnation pressures. The structural model representing a wind tunnel model is built in a two-step process. Firstly, the complete volume of the wing is meshed with six-sided and five-sided solid elements, all having the same material properties of a maraging steel. By performing a normal modes analysis in MSC.Nastran (SOL103) with the wing root rigidly clamped, the mode shapes and eigenfrequencies are identified disregarding structural damping.

Secondly, the structural model is artificially weakened by introducing reduction factors for each eigenfrequency to obtain a flutter case. The first eigenfrequency is reduced less to provide a reasonable upper bound on the required simulation time. The thus obtained first ten eigenmodes are used in the CFD-CSM coupling. Table 1 lists the reduction factors and baseline eigenfrequencies together with a description of the associated mode shapes.

Table 1. Structural model: mode shapes and wind-off eigenfrequencies

Mode	Description	f/Hz	Mode	Description	f/Hz
1	1^{st} bending	$0.5 \cdot 17.84$	6	4^{th} bending	$0.25 \cdot 250.32$
2	2^{nd} bending	$0.25 \cdot 60.14$	7	2^{nd} torsion	$0.25 \cdot 351.36$
3	3^{rd} bending	$0.25 \cdot 137.39$	8	5^{th} bending	$0.25 \cdot 398.31$
4	1^{st} in-plane	$0.25 \cdot 161.93$	9	2^{nd} in-plane	$0.25 \cdot 507.85$
5	1^{st} torsion	$0.25 \cdot 193.39$	10	3^{rd} torsion	$0.25 \cdot 527.29$

3.3 Aeroelasticity

For each Mach number, coupled CFD-CSM computations are performed to determine the largest structural deformation at a given freestream pressure. At the Mach number that results in the largest deformation, the freestream pressure is varied to determine the critical pressure, for which flutter occurs with a step size of $\Delta p = 0.2$ bar.

The largest deformations are found for $M = 0.82$. The steady flow condition is shown in Fig. 6 at two span stations in terms of the pressure and skin friction coefficient distribution. For the transitional flow, a shock-induced boundary layer separation covers the whole wing span. The fully turbulent flow only separates in the outer wing section (outboard of $\eta = y/(b/2) = 0.55$) as the shock is weaker and the turbulent boundary layer is less prone to separate.

Figure 7 and 8 show the modal coordinates of the first six eigenmodes (compare Table 1) at the critical pressure. The flutter instability occurs at a lower

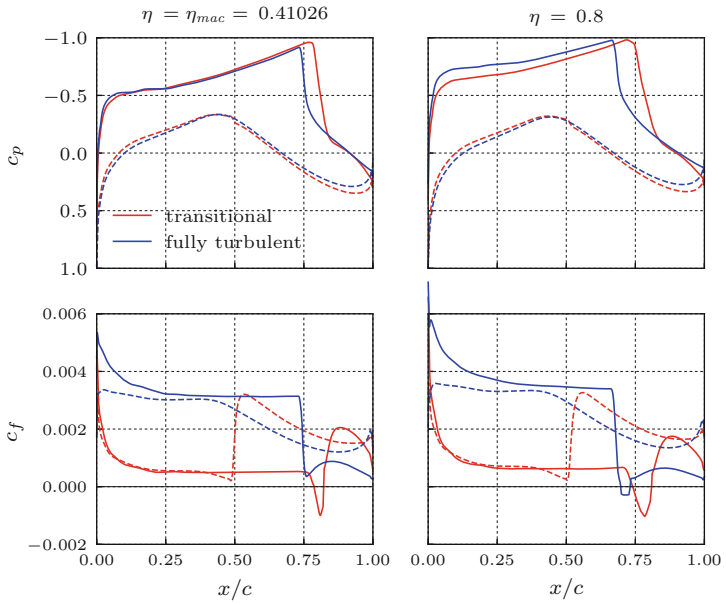

Fig. 6. DLR-AE-L1 Wing: pressure and skin friction coefficient distribution at $M = 0.82$, $C_L = 0.5$, $Re = 15 \cdot 10^6$; full line: upper surface, dashed line: lower surface

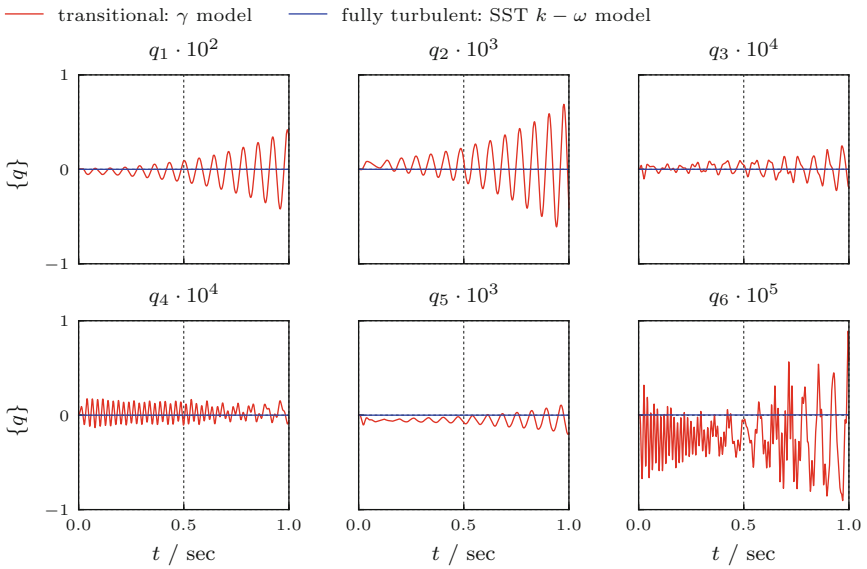

Fig. 7. DLR-AE-L1 Wing: modal coordinate q of the first 6 eigenmodes for $p = 2$ bar

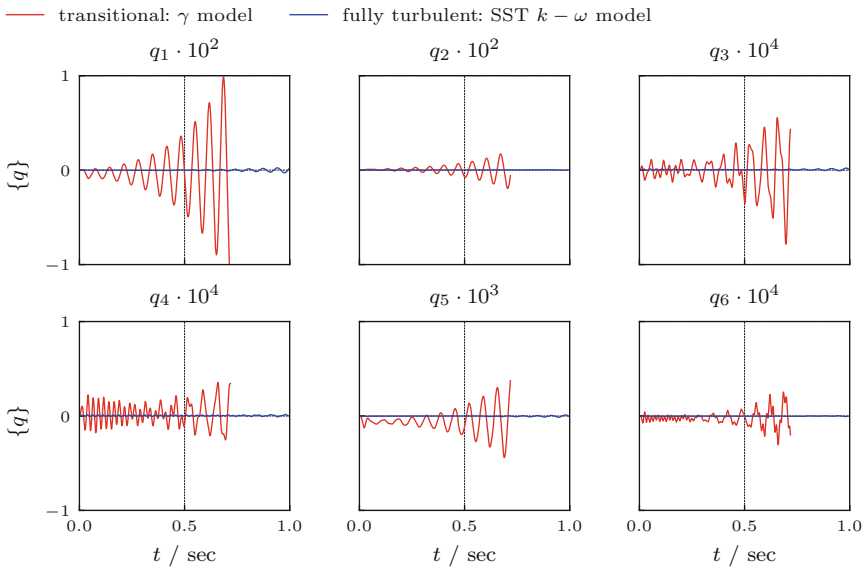

Fig. 8. DLR-AE-L1 Wing: modal coordinate q of the first 6 eigenmodes for $p = 2.2$ bar

pressure of $p = 2$ bar in the transitional flow compared to $p = 2.2$ bar in a fully turbulent flow. Table 2 gives the flutter frequency f_{fl} and the logarithmic decrement $\Lambda = \ln(\widehat{q}_n/\widehat{q}_{n+1})$ defined by two consecutive oscillation maxima $\widehat{q}$ obtained from mode 1. Although the flutter mode is the same for both flow conditions, the transitional flow is more severe in terms of critical pressure and mode excitation. In the case of the transitional flow at $p = 2.2$ bar, the computation is terminated as the grid deformation fails for larger oscillations.

Table 2. Flutter frequency f_{fl} and logarithmic decrement Λ obtained from mode 1

	Transitional		Fully turbulent	
p/bar	f_{fl}/Hz	Λ	f_{fl}/Hz	Λ
2.0	14.306	−0.191		
2.2	14.846	−0.328	14.791	−0.284

To put the resulting modal displacements into perspective, Fig. 9 and 10 show the time history of the lift and moment coefficient. For reference, a quasi-steady lift increase of $\Delta C_L = 0.01$ is found for an angle of attack increase of $\Delta\alpha \approx 0.067°$ for the transitional flow neglecting any unsteady effects.

A time step size of $\mathrm{d}t = 2.62 \cdot 10^{-4}$ s is used for all unsteady computations, for which the inner iterations converge sufficiently well. The spatial and temporal discretization is based on experience for computations with similar flow

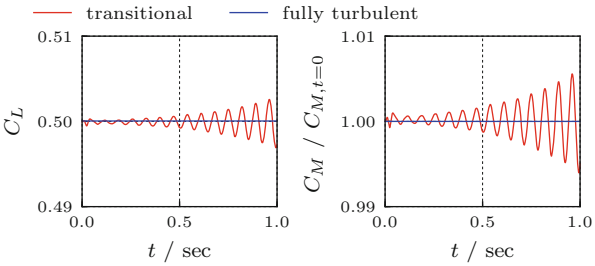

Fig. 9. DLR-AE-L1 Wing: lift and moment coefficient for $p = 2$ bar

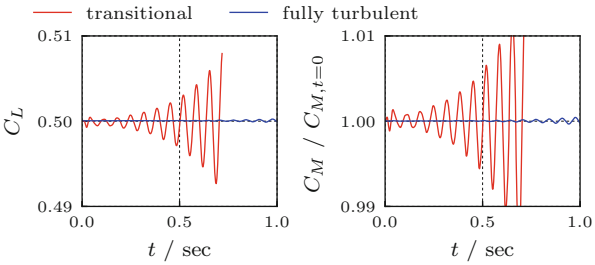

Fig. 10. DLR-AE-L1 Wing: lift and moment coefficient for $p = 2.2$ bar

conditions. However, the grid and time step size need to be put under scrutiny in future studies. In addition, a longer time span needs to be covered to investigate the occurrence of limit cycle oscillations.

4 Conclusion and Outlook

At the moment, there is no proof that a partly laminar boundary layer flow in transonic flow is necessarily more critical in terms of its aeroelastic behavior compared to a fully turbulent flow. However, this research supports the observation that aerodynamic forces in a transitional flow change in a way, that facilitates the occurrence of dynamic instabilities in the transonic flight regime. A more detailed investigation of the character of transitional transonic flutter is required and will be carried out. In addition, a detailed description of the unsteady aerodynamics associated with each structural mode is needed to understand differences between the fully turbulent and transitional flutter behavior. As the numerical computations are only bound by numerical stability and not by any actual structural properties, the occurrence of limit cycle oscillations is likely and the limiting mechanisms need to be described and understood.

More general, two important fields of research emerge for future work: First, the aeroelastic effects in a transitional, unsteady transonic flow need to be understood through wind tunnel experiments and numerical studies. Second, transition modeling approaches need to be placed under scrutiny to develop a sound model

representation, that captures boundary layer transition in unsteady flows and complex shock boundary layer interaction.

Acknowledgments. This work was funded within the DLR project VicToria.

References

1. Tichy, L., Mai, H., Fehrs, M., Nitzsche, J., Hebler, A.: Risk analysis for flutter of laminar wings. In: IFASD, IFASD-2017-196, Como (2017)
2. Seitz, A., Hübner, A., Risse, K.: The DLR TuLam project: design of a short and medium range transport aircraft with forward swept NLF wing. CEAS Aeronaut. J. **11**, 449–459 (2020)
3. Lynde, M.N., Campbell, R.L.: Computational design and analysis of a transonic natural laminar flow wing for a wind tunnel model. In: 35th AIAA Applied Aerodynamics Conference, AIAA 2017-3058, Denver (2017)
4. Klimmek, T.: Parameterization of topology and geometry for the multidisciplinary optimization of wing structures. In: Proceedings CEAS 2009 - European Air and Space Conference, Manchester (2009)
5. Schwamborn, D., Gerhold, T., Heinrich, R.: The DLR TAU-code: recent applications in research and industry. In: Proceedings European Conference on Computational Fluid Dynamics ECCOMAS, TU Delft, Delft (2006)
6. Fehrs, M.: Boundary layer transition in external aerodynamics and dynamic aeroelastic stability. Dissertation, TU Braunschweig (2018). ISSN 1434–8454, ISRN DLRFB-2018-11, also NFL-FB 2017–27, Braunschweig (2018)
7. Krumbein, A., Krimmelbein, N., Schrauf, G.: Automatic transition prediction in hybrid flow solver, part 1: methodology and sensitivities. J. Aircr. **46**(4), 1176–1190 (2009)
8. Krumbein, A., Krimmelbein, N., Schrauf, G.: Automatic transition prediction in hybrid flow solver, part 2: practical application. J. Aircr. **46**(4), 1191–1199 (2009)
9. Reimer, L.: The FlowSimulator - a software framework for CFD-related multidisciplinary simulations. In: European NAFEMS Conference: Computational Fluid Dynamics (CFD) - Beyond the Solve, München (2015)
10. Newmark, N.M.: A method of computation for structural dynamics. J. Eng. Mech. ASCE **85**(EM3), 67–94 (1959)
11. Versteegh, T.C.: Natural laminar flow, low wave drag airfoil. European Patent Office. EP0111785A1, status: withdrawn (1983)